

# Kinetic Model for $\text{Ca}^{2+}$ -induced Permeability Transition in Energized Liver Mitochondria Discriminates between Inhibitor Mechanisms\*

Received for publication, April 26, 2007, and in revised form, September 19, 2007. Published, JBC Papers in Press, October 25, 2007, DOI 10.1074/jbc.M703484200

Sergei V. Baranov<sup>‡§</sup>, Irina G. Stavrovskaya<sup>‡§</sup>, Abraham M. Brown<sup>§¶</sup>, Alexei M. Tyryshkin<sup>||</sup>, and Bruce S. Kristal<sup>‡§¶\*</sup>

From the <sup>‡</sup>Department of Neurosurgery, Brigham and Women's Hospital, Boston, Massachusetts 02115, <sup>§</sup>Burke Medical Research Institute, White Plains, New York 10605, the <sup>¶</sup>Department of Biochemistry and <sup>\*\*</sup>Department of Neuroscience, Cornell University Medical College, New York, New York 10021, the <sup>||</sup>Department of Electrical Engineering, Princeton University, Princeton, New Jersey 08544

Cytotoxicity associated with pathophysiological  $\text{Ca}^{2+}$  overload (e.g. in stroke) appears mediated by an event termed the mitochondrial permeability transition (mPT). We built and solved a kinetic model of the mPT in populations of isolated rat liver mitochondria that quantitatively describes  $\text{Ca}^{2+}$ -induced mPT as a two-step sequence of pre-swelling induction followed by  $\text{Ca}^{2+}$ -driven, positive feedback, autocatalytic propagation. The model was formulated as two differential equations, each directly related to experimental parameters ( $\text{Ca}^{2+}$  flux/mitochondrial swelling). These parameters were simultaneously assessed using a spectroscopic approach to monitor multiple mitochondrial properties. The derived kinetic model correctly identifies a correlation between initial  $\text{Ca}^{2+}$  concentration and delay interval prior to mPT induction. Within the model's framework, Ru-360 (a ruthenium complex) and  $\text{Mg}^{2+}$  were shown to compete with the  $\text{Ca}^{2+}$ -stimulated initiation phase of mPT induction, consistent with known inhibition at the phenomenological level of the  $\text{Ca}^{2+}$  uniporter. The model further reveals that  $\text{Mg}^{2+}$ , but not Ru-360, inhibits  $\text{Ca}^{2+}$ -induced effects on a downstream stage of mPT induction at a site distinct from the uniporter. The analytical approach was then applied to promethazine, an FDA-approved drug previously shown to inhibit both mPT and ischemia-reperfusion injury. Kinetic analysis revealed that promethazine delayed mPT induction in a manner qualitatively distinct from that of lower concentrations of  $\text{Mg}^{2+}$ . In summary, we have developed a kinetic model to aid in the quantitative characterization of mPT induction. This model is consistent with/informative about the biochemistry of several mPT inhibitors, and its success suggests that this kinetic approach can aid in the classification of agents or targets that modulate mPT induction.

Cytotoxicity resulting from pathological insults, such as cardiac ischemia-reperfusion injury, stroke (1), and excitotoxicity (2, 3), is known to involve both pathophysiological rises in intra-

cellular  $\text{Ca}^{2+}$  concentration and a mitochondria-associated process. These events have been hypothesized to be linked biochemically, because mitochondria are a major site for  $\text{Ca}^{2+}$  sequestration, normally absorbing excess cytosolic  $\text{Ca}^{2+}$  through the  $\text{Ca}^{2+}$  uniporter (which is driven by the membrane potential  $\Delta\varphi_m$ )<sup>2</sup> and releasing it via the  $\text{Na}^+/\text{Ca}^{2+}$  and  $\text{Ca}^{2+}/\text{H}^+$  exchangers, resulting in a slow, continuous cycling of  $\text{Ca}^{2+}$  across the inner mitochondrial membrane. Experiments in multiple laboratories have provided evidence that a specific mitochondrial event triggered by  $\text{Ca}^{2+}$ -overload, the mitochondrial permeability transition (mPT), might play causative roles in cell death in the presence of the above and other pathological insults (4–7). These and related studies have further suggested that inhibition of the mPT might have potential therapeutic utility.

The mPT has been classically defined in isolated liver mitochondria as the cyclosporin A-sensitive,  $\text{Ca}^{2+}$ -mediated formation/opening of an mPT pore (mPTP) in the inner mitochondrial membrane, allowing free diffusion of water and solutes under 1500 daltons and subsequent large amplitude swelling of mitochondria and release of their sequestered  $\text{Ca}^{2+}$  (8–11). From a kinetic point of view, at least three conceptually distinct phases must be resolved during the mPT induction: (i) the initiation phase, which includes the initial intake of excess  $\text{Ca}^{2+}$  via the  $\text{Ca}^{2+}$  uniporter; (ii) the “lag” phase, during which  $\text{Ca}^{2+}$  cycling induces or accompanies a series of reactions in mitochondria (e.g. the pore constituents are recruited and possibly assembled); and (iii) the propagation or termination phase. This final phase is associated with a decrease in membrane potential observable at the population level, release of mitochondrially sequestered  $\text{Ca}^{2+}$  (and a resultant increase in the steady-state  $\text{Ca}^{2+}$  concentration in the medium, which consequently fuels subsequent  $\text{Ca}^{2+}$  uptake by the remaining intact mitochondria, creating a positive feedback loop for damage propagation), final pore assembly, and pore opening. These events result in the loss of integrity of the inner mitochondrial

\* This work was supported by a New York State CORE Grant (to R. Ratan (Director) and B. S. K. (Project Leader)) and funds from the Department of Neurosurgery, Brigham and Women's Hospital. The costs of publication of this article were defrayed in part by the payment of page charges. This article must therefore be hereby marked “advertisement” in accordance with 18 U.S.C. Section 1734 solely to indicate this fact.

<sup>1</sup> To whom correspondence should be addressed: Dept. of Neurosurgery, Brigham and Women's Hospital, 221 Longwood Ave., LM322B, Boston, MA 02115. Tel.: 617-525-3280; Fax: 617-264-6862; E-mail: bkristal@partners.org.

<sup>2</sup> The abbreviations used are:  $\Delta\varphi_m$ , mitochondrial membrane potential; mPT, mitochondrial permeability transition; mPTP, nPT pore; TMRM, tetramethylrhodamine methyl ester;  $\Delta[\text{Ca}^{2+}]$ , change(s) in  $\text{Ca}^{2+}$  concentration;  $[\text{MH}]_A$ , a population of active, unswollen mitochondria;  $[\text{MH}]_I$ , an intermediate state;  $[\text{MH}]_S$ , a population of inactive (swollen) mitochondria;  $[\text{Ca}^{2+}]_T$ ,  $\text{Ca}^{2+}$  added to the assay medium;  $[\text{Ca}^{2+}]_{\text{out}}$ , extramitochondrial  $\text{Ca}^{2+}$ ;  $[\text{Ca}^{2+}]_M$ ,  $\text{Ca}^{2+}$  absorbed by mitochondria.

membrane, uncoupling of oxidative phosphorylation, and mitochondrial swelling. Notably, at least under conditions in which the concentration of added  $\text{Ca}^{2+}$  is relatively low, the termination phase appears to be very short relative to the lag phase when considered at the population level (*i.e.* at the level typically observed experimentally). Thus, we do not further consider the termination phase in our kinetic model.

Thus, the mPT induction may be kinetically described (under low  $\text{Ca}^{2+}$  conditions only) as having only two phases, the initiation phase and the lag phase, where the latter is described as the period after the initiation phase and before mitochondrial swelling. In this model, the actual swelling event (step iii above) is all-or-none and takes place nearly instantaneously for each individual mitochondrial particle. Both the initiation and lag phases are complex reactions that involve a multitude of parallel and interrelated processes (*e.g.* calcium cycling, pyridine nucleotide oxidation, oxidation of other compounds, membrane changes, etc.). Systematic kinetic studies should allow valuable insight into details of these processes and, in particular, how they are altered by compounds or conditions that modulate mPT induction.

Interpretation of kinetic data requires an appropriate kinetic model. There are two conceptually distinct (and complementary) approaches to building useful kinetic models of mPT induction. One approach leans heavily on theory and *a priori* knowledge of the molecular processes during the mPT induction and attempts to describe it in the greatest possible detail by accounting for all physico-chemical and biochemical processes, including, but not limited to,  $\text{Ca}^{2+}$  homeostasis, mitochondrial respiration, substrate transfer, energy utilization, substrate concentrations, and cofactor concentrations. To our knowledge, the most comprehensive attempt in this direction was made by Pokhilko *et al.* (12). The utility of any model of this class, however, is intrinsically limited by our current lack of sufficiently detailed information and knowledge about the system and all of its components and their interactions. An alternative approach, which is utilized in the present work, is to build an empirical kinetic model that involves a minimal number of parameters and yet is capable of describing the experimental kinetic data (*i.e.* a “minimal kinetic model”). Massari (13) used a simple, first order kinetic model to describe the swelling of mitochondria subsequent to exposure to phenylarsine oxide, a strong thiol oxidant, or to high levels of calcium. Krasnikov *et al.* (14) expanded this analysis to describe parameters other than swelling but otherwise retained the first order kinetic model developed by Massari (13) and did not utilize information from multiple data acquisition channels. However, the first order kinetic models developed by Massari (13) and used by Krasnikov *et al.* (14) are only applicable at saturating concentrations of  $\text{Ca}^{2+}$  and fail to account for the lag phase often observed at lower, more (patho)physiologically relevant  $\text{Ca}^{2+}$  concentrations.

The present study formulates a “minimal kinetic model” of the mPT that involves a minimal number of parameters (*i.e.* the number of parameters in the model cannot be reduced without loss of information) so as to reduce complexity and reduce the possibility of “overfitting” the data. The model is based on the data obtained from experimental studies of isolated rat liver

mitochondria and defines the intrinsic rates of change that describe the coordinated changes in  $\text{Ca}^{2+}$  concentration in the assay medium ( $[\text{Ca}^{2+}]_{\text{out}}$ ) and swelling. Specifically, we simultaneously measured the kinetic evolution of these two parameters during the mPT and then used these data as the basis for our model.  $\text{Ca}^{2+}$  fluxes and swelling were chosen because they are established indicators of mPT induction in liver mitochondria. The model was formulated as a set of simultaneous differential equations that can be solved numerically to fit the experimental kinetics. The model is shown to describe the  $\text{Ca}^{2+}$ -induced mPT quantitatively as a two-step reaction in energized mitochondria and makes accurate predictions about linear relationships between levels of modulators of the mPT and parameters of mPT induction. In this report, we begin by modeling a specific case, a pure  $\text{Ca}^{2+}$  overload model of the mPT. We will then show that the model can be easily generalized to more complex situations, such as when additional mPT modulators (*e.g.* inhibitors and inducers) are present. The results from different modifiers (*e.g.* promethazine,  $\text{Mg}^{2+}$ , ruthenium red) suggest that these modifiers interact with different targets and provide insights into potential mechanisms or sites of action.

## EXPERIMENTAL PROCEDURES

**Chemicals**—Fluorescent probes were purchased from Invitrogen and stored according to the manufacturer’s instructions. All other chemicals were obtained from Sigma and were of the highest purity available.

**Mitochondrial Isolation**—Liver mitochondria were isolated from 4–6-month-old male Fischer 344 X Brown Norway  $F_1$  rats by differential centrifugation using sucrose-based buffers (14–16).

**Assays of Mitochondrial Function**—Mitochondrial experiments were carried out using a buffer containing 250 mM sucrose, 10 mM HEPES, 5 mM succinate (added as succinic acid), 1 mM  $\text{KH}_2\text{PO}_4$ , and 2.5  $\mu\text{M}$  EDTA adjusted to pH 7.4 with KOH. In all cases, isolated mitochondria were added to a concentration of 0.25 mg of protein/ml. We note that the sensitivity of the fluorimeter described below allowed reliable measurement of the basic mitochondria parameters even at protein concentrations as low as 0.05 mg/ml.

Fluorescent dyes, including TMRM (0.06  $\mu\text{M}$ ) and Ca-Green-5N (0.3  $\mu\text{M}$ ), were used to simultaneously measure  $\Delta\varphi_m$  and  $[\text{Ca}^{2+}]_{\text{out}}$ , respectively. Based on known spectroscopic properties of TMRM (17), we measured changes in dye fluorescence yield using an excitation wavelength of 546 nm and emission at 590 nm. Quenching of the fluorescence has been attributed to binding of TMRM to the mitochondrial membranes. Therefore, loss of fluorescence indicates increased potential-dependent binding of TMRM. Conversely, reduced  $\Delta\varphi_m$  results in release of bound TMRM and increased fluorescent signal. For the purpose of the experiments reported here, TMRM was used only as a qualitative indicator and was not directly considered in our kinetic model. The increase of Ca-Green-5N fluorescence caused by complex formation with extramitochondrial  $\text{Ca}^{2+}$  (18) was monitored using an excitation/emission pair ( $\lambda_{\text{ex/em}}$ ) of 488/535 nm, respectively. Mitochondrial swelling and NAD(P)H oxidation were also simulta-

neously measured as changes of light scattering at  $\lambda_{\text{ex/em}} = 587$  nm and changes in fluorescence at  $\lambda_{\text{ex/em}} = 377/440$  nm, respectively.

Simultaneous measurement of  $\text{Ca}^{2+}$  fluxes, mitochondrial  $\Delta\varphi_m$ , mitochondrial swelling, and changes in NAD(P)H oxidation were done using a multichannel wheel-based fluorimeter. The set-up was equipped with a temperature-controlled quartz cuvette (optical pathway = 1 cm) and stirrer. Paired excitation/emission filters provide precision comparable with that of monochromator-based fluorescence spectrometers. A full description of the experimental set-up is available on the Web site of the manufacturer, C&L instruments.

**Mitochondria Swelling and NAD(P)H Calibration**—As discussed below, our minimal kinetic model of  $\text{Ca}^{2+}$ -induced mPT assumes that mitochondria can exist in one of two states: either with mPTP closed (so that mitochondria are not swollen) or mPTP opened (so that mitochondria are swollen). To quantitatively determine what fraction of mitochondria were swollen in kinetic experiments required accurate calibration of the fluorescence system. To obtain a fully swollen fraction, mitochondria were incubated for at least 15 min at 30 °C in the presence of high concentrations of  $\text{CaCl}_2$  (50  $\mu\text{M}$ ). Then an excess of EGTA was added to remove free  $\text{Ca}^{2+}$ . Another sample of mitochondria was incubated in parallel in the same medium without  $\text{Ca}^{2+}$  and with added EGTA to suppress mPT. The intact and swollen mitochondrial samples were mixed in different proportions, and their light scattering properties as well as the autofluorescence of mitochondrial NAD(P)H were measured. After each measurement, the nonspecific pore-forming agent alamethicin was added to the sample in order to ensure full-scale swelling of each sample (Fig. 1A, inset). The signal obtained after the addition of alamethicin was then subtracted from the initial fluorescence readings. Thus, the difference in fluorescence obtained from the control sample (*i.e.* the sample incubated in  $\text{Ca}^{2+}$ -free medium) before and after the addition of alamethicin represents the maximal fluorescence yield associated with mitochondrial swelling. The intermediate values of fluorescence yield were then plotted *versus* the percentage of swollen mitochondrial present in the sample to provide a calibrated curve. As shown in Fig. 1A, the values obtained for swollen mitochondria as well as for NAD(P)H were linearly proportional to the fractional content of intact mitochondria in the sample across the full range of optical properties examined in our experiments. We note that the mitochondria in the sample that initially contained 100% swollen mitochondria underwent further changes in scattering (about 5%) after the addition of alamethicin. This additional swelling, however, did not affect our kinetic analysis, although the absolute values of the percentage of mitochondria that have undergone a mPT may be slightly inaccurate because of this phenomenon if it reflects mitochondria that did not undergo mPT as opposed to swelling related specifically to alamethicin-induced pore formation.

**Calibration of the  $\text{Ca}^{2+}$  Signal Channel**—To calibrate the  $\text{Ca}^{2+}$  channel, known amounts of  $\text{CaCl}_2$  were sequentially added to the assay medium, and the  $\text{Ca}^{2+}$  signal was measured as the change in Ca-Green-5N fluorescence. The assay medium contained all of the compounds that were used during the actual kinetic experimental series as well as mitochondria swol-

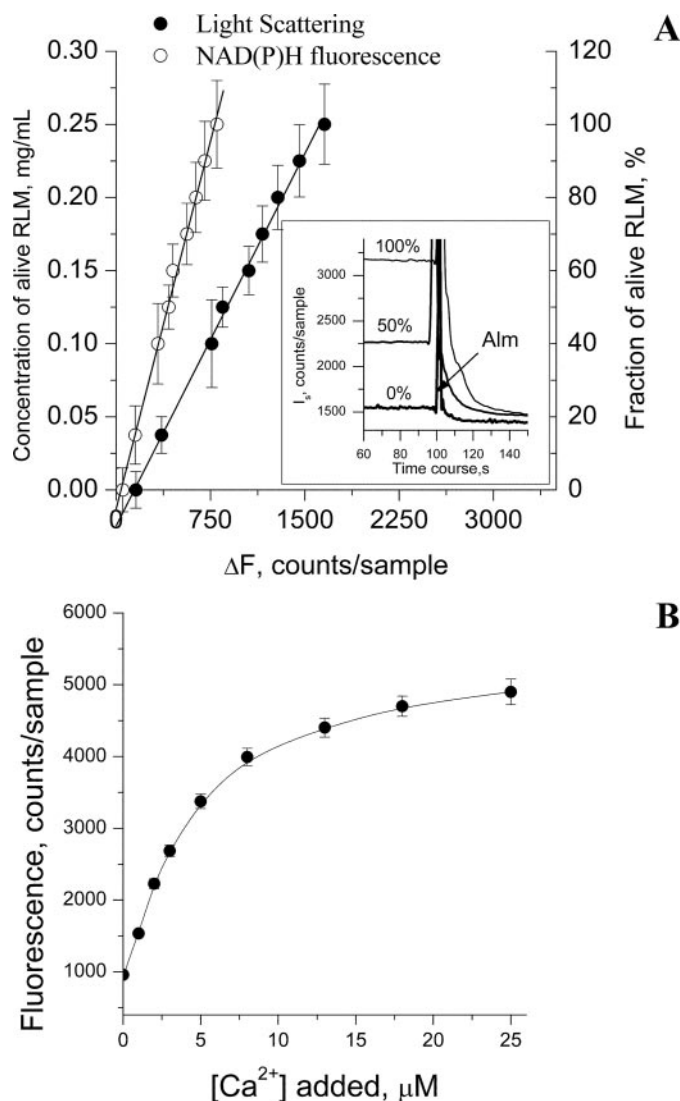


FIGURE 1. A, dependence of optical properties of mitochondria on the fraction of swollen mitochondria. Solid circles, swelling of mitochondria measured as light scattering at 587 nm. Open circles, level of NAD(P)H oxidation measured as autofluorescence of mitochondrial pyridine nucleotides at  $\lambda_{\text{ex/em}} = 340/377$  nm. The inset represents typical changes in optical properties of a suspension of unswollen mitochondria mixed with swollen (at ratios of 100, 50, and 0%) upon the addition of alamethicin (Alm). For a detailed description, see "Experimental Procedures." RLM, rat liver mitochondria. B, plot of Ca-Green-5N fluorescence yield *versus* calcium concentration in the assay medium measured at  $\lambda_{\text{ex/em}} = 480/535$  nm. Measurements were done in the assay medium, which contained 250 mM sucrose, 10 mM HEPES, 5 mM potassium succinate, 1 mM  $\text{KH}_2\text{PO}_4$ , 2.5  $\mu\text{M}$  EDTA, and 0.3  $\mu\text{M}$  Ca-Green-5N adjusted to pH 7.4 with KOH. The measurements were done in the presence of mitochondria (0.25 mg of protein/ml) swollen with alamethicin. The graphs represent results from at least three independent measurements for each point; the S.D. value is plotted as error bars.

len by the addition of alamethicin. The inclusion of mitochondria during calibration helped account for changes in optical properties (light scattering) of the assay medium that we could not otherwise account for, given our use of nonratiometric dyes. The calibration curve, shown in Fig. 1B, was used to scale changes in fluorescence of Ca-Green-5N during the experimental series. Ca-Green is commonly used as a  $\text{Ca}^{2+}$  probe, but it also possesses affinity to other divalent cations, such as  $\text{Mg}^{2+}$ . To account for this secondary affinity, we also calibrated the

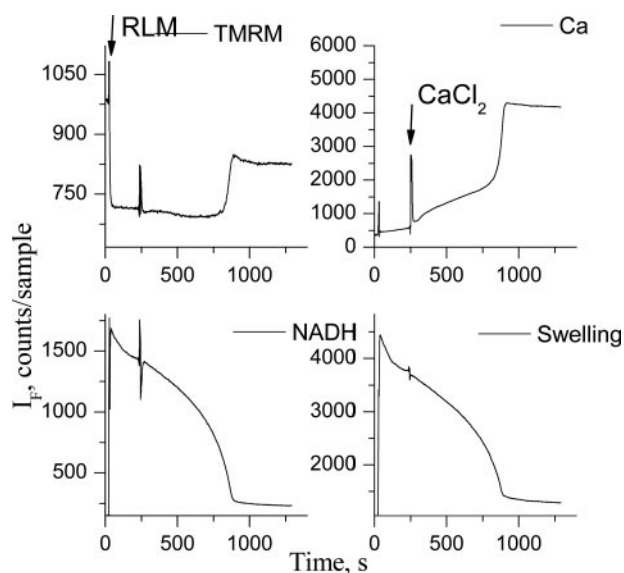


FIGURE 2. Simultaneous measurements of four mitochondrial parameters in typical experiments. TMRM,  $\text{Ca}^{2+}$ , NADH, and Swelling represent changes in  $\Delta\varphi_m$ , extramitochondrial  $\text{Ca}^{2+}$  concentration, NAD(P)H fluorescence, and light scattering, respectively. Time of the addition of mitochondria (0.25 mg/ml) and calcium (10  $\mu\text{M}$ ) are shown by arrows. The assay medium contained 250 mM sucrose, 10 mM HEPES, 5 mM potassium succinate, 1 mM  $\text{KH}_2\text{PO}_4$ , and 2.5  $\mu\text{M}$  EDTA, adjusted to pH 7.4 with KOH. 0.3  $\mu\text{M}$  Ca-Green-5N and 60 nM TMRM were used to assign extramitochondrial  $[\text{Ca}^{2+}]$  and  $\Delta\varphi_m$ , respectively. RLM, rat liver mitochondria.

$\text{Ca}^{2+}$  signal channel with solutions containing each of the  $\text{Mg}^{2+}$  concentrations used in our experiments.

## RESULTS

**Kinetic Model of  $\text{Ca}^{2+}$ -induced mPT**—Four parameters ( $\text{Ca}^{2+}$  concentration, membrane potential  $\Delta\varphi_m$ , concentration of reduced pyridine nucleotides (NAD(P)H), and 90° light scattering (which reflects mitochondria swelling)) were simultaneously measured in our experiments. Induction of mPT by the addition of  $\text{Ca}^{2+}$  was observed in the experiments as  $\text{Ca}^{2+}$  release and swelling of the mitochondria. Typical raw kinetic curves for all four parameters obtained upon the addition of 10  $\mu\text{M}$   $\text{Ca}^{2+}$  are shown in Fig. 2. The data on  $\text{Ca}^{2+}$  concentration, reduced pyridine nucleotides (NAD(P)H), and mitochondrial swelling were then rescaled using the calibration curves from Fig. 1 (see Fig. 3). In all experiments presented in this report, the kinetics for the swelling and NAD(P)H channels were equivalent. We therefore discuss only swelling data from this point on. We note, however, that other agents may uncouple these signals and that one or the other or both signals may later be shown to be preferential in some or all situations. We also do not discuss further the changes in  $\Delta\varphi_m$  as a stand-alone variable in the context of our current model, because the experimental set-up used was not optimized for quantitative estimation of  $\Delta\varphi_m$ . Thus, in the analysis that follows, only the kinetic data for  $\text{Ca}^{2+}$  concentration and mitochondria swelling were used to formulate the kinetic model of the mPT process.

The kinetic curve for mitochondria swelling (Fig. 3, bottom right) reveals a monotonic decay, and the rate of decay accelerates noticeably with time. The  $\text{Ca}^{2+}$  concentration in the buffer (Fig. 3, top right) is clearly correlated with the mitochondrial swelling curve; however, this correlation is nontrivial and kinet-

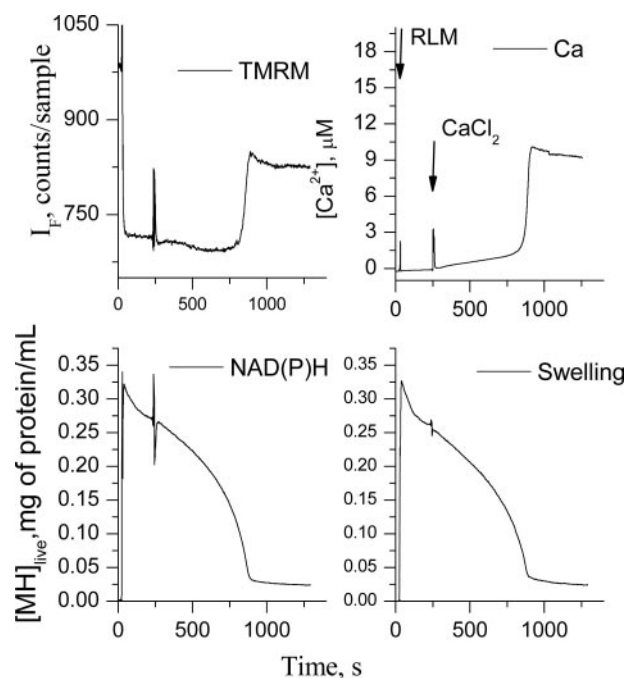
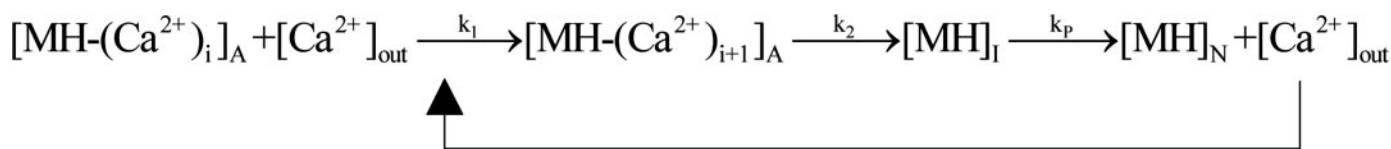


FIGURE 3. Scaled measurements of mitochondrial parameters shown in Fig. 2.  $\text{Ca}^{2+}$ , NAD(P)H, and Swelling channels were rescaled in accordance with the calibration measurements shown in Fig. 1. RLM, rat liver mitochondria.

ically complex. Within the first 10–20 s after the addition of  $\text{Ca}^{2+}$  to the medium (10  $\mu\text{M}$   $\text{Ca}^{2+}$  were added in Fig. 3), the  $\text{Ca}^{2+}$  concentration dropped quickly to a submicromolar level, indicating that most of the added  $\text{Ca}^{2+}$  was immediately absorbed by mitochondria. This absorbed  $\text{Ca}^{2+}$  initiated the mPT reaction. During the next 600 s, the fraction of “active” mitochondria (*i.e.* the fraction of mitochondria capable of electrogenic  $\text{Ca}^{2+}$  uptake) progressively decreased (albeit very slowly during this phase), and the fraction of swollen mitochondria slowly increased. The swollen mitochondria released their absorbed  $\text{Ca}^{2+}$  back to the medium through the opened mPTP, but the concentration of free  $\text{Ca}^{2+}$  in the medium increased more slowly than the population of swollen mitochondria, because the released  $\text{Ca}^{2+}$  was immediately reabsorbed by other active mitochondria. This secondary reabsorption of  $\text{Ca}^{2+}$  resulted in an elevated concentration of absorbed  $\text{Ca}^{2+}$  in the still active mitochondria that in turn resulted in their accelerated swelling rate, as shown in Fig. 3. The full concentration of  $\text{Ca}^{2+}$  was recovered back into the medium only at the end of the mPT reaction when all mitochondria were swollen.

To account for this  $\text{Ca}^{2+}$  reabsorption phenomenon and its accelerating effect on the rate of the mPT process, we propose the kinetic model shown in Scheme 1, where  $[\text{MH}-(\text{Ca}^{2+})_i]_A$  represents a population of active, unswollen mitochondria ( $[\text{MH}]_A$ ), and  $i$  represents the number of  $\text{Ca}^{2+}$  already adsorbed by a given mitochondria.  $\text{Ca}^{2+}$  absorption occurs during the  $k_1$  step shown in the scheme as formation of  $[\text{MH}-(\text{Ca}^{2+})_{i+1}]_A$ , and it initiates the mPT process that we describe here as a sequence of two steps. The  $k_2$  step is a rate-limiting step of the mPT induction that results in the formation of the intermediate state  $[\text{MH}]_I$ . The next step ( $k_p$ ) leads to the formation of a population of inactive (swollen) mitochondria, represented as  $[\text{MH}]_N$ , with all  $\text{Ca}^{2+}$  released back to the medium.  $[\text{Ca}^{2+}]_{\text{out}}$  is



SCHEME 1. Kinetic model of the mPT.

the concentration of free  $\text{Ca}^{2+}$  in the medium, available for absorption by mitochondria. Now we can define  $\text{Ca}^{2+}$  absorbed by mitochondria ( $[\text{Ca}^{2+}]_M$ ) as the product of a number ( $i$ ) of absorbed  $\text{Ca}^{2+}$  and concentration of “active” mitochondria,  $[\text{MH}]_A$  (i.e.  $[\text{Ca}^{2+}]_M = i \times [\text{MH}]_A$ ). It is assumed that total concentration of  $\text{Ca}^{2+}$  (e.g.  $[\text{Ca}^{2+}]_T = [\text{Ca}^{2+}]_{\text{out}} + [\text{Ca}^{2+}]_M$ ) is constant during the reaction (i.e. there is a single addition, after which no further  $\text{Ca}^{2+}$  is added). This model involves a number of assumptions that are introduced to reflect specific characteristics of the mPT process. These assumptions are as follows. (i)  $\text{Ca}^{2+}$  uptake is a bimolecular reaction with rate constant  $k_1$ . In other words, the rate of  $\text{Ca}^{2+}$  uptake is a product  $k_1 \times [\text{MH}]_A \times [\text{Ca}^{2+}]_{\text{out}}$  and thus can change during the course of the reaction in proportion with  $[\text{MH}]_A$  and  $[\text{Ca}^{2+}]_{\text{out}}$ . The apparent rate constant ( $k_1$ ) is a complex function that subsumes many processes that are associated with  $\text{Ca}^{2+}$  sequestering in mitochondria and that include  $\text{Ca}^{2+}$  influx and  $\text{Ca}^{2+}$  release mechanisms. In this model, we assume that all active mitochondria are equally capable of absorbing the  $\text{Ca}^{2+}$ , and, under the conditions used, their absorption rate ( $k_1$ ) is essentially (mathematically) independent of the amount of  $\text{Ca}^{2+}$  already absorbed by the given mitochondria. This latter assumption appears valid under the  $\text{Ca}^{2+}$  conditions used in this study. (ii) The rate of formation of the intermediate state  $[\text{MH}]_I$  is a complex function of the number of  $\text{Ca}^{2+}$  ions absorbed by the mitochondria.

$$k_2 = k'_2 \times ([\text{Ca}^{2+}]_M / [\text{MH}]_A)^n \quad (\text{Eq. 1})$$

Here  $[\text{Ca}^{2+}]_M$  is the concentration of  $\text{Ca}^{2+}$  that has been absorbed by mitochondria; thus, the ratio  $[\text{Ca}^{2+}]_M / [\text{MH}]_A$  is essentially an average number of  $\text{Ca}^{2+}$  ions absorbed per active mitochondrion.  $n$  is an apparent order of the  $k_2$  step with respect to  $\text{Ca}^{2+}$ , and  $k'_2$  is a reaction constant of this step. mPT induction is a complex chain of interconnected reactions triggered by  $\text{Ca}^{2+}$ ; therefore, describing this complex step with one rate constant (e.g.  $k_2$ ) may be an oversimplification. Our rationale for this oversimplification is that in any complex chain of reactions, there always must be one reaction that is the slowest and thus determines the overall rate (ignoring, for the purpose of this modeling exercise, the situation in which multiple steps have control coefficients  $>0$  and  $<1$  (i.e. reactions in which there are multiple partially limiting reactions or when the time frame of the  $k_2$  step becomes comparable with or less than that of the  $k_p$  step). The apparent order  $n$  is closely related to the  $\text{Ca}^{2+}$  order of this slowest reaction, and  $k'_2$  is a rate constant of this slowest step. In principal,  $n$  can be a noninteger number, because it can be affected by other reactions in the chain, including, but not limited to, mitochondrial heterogeneity,  $\text{Ca}^{2+}$  buffering capacity of energized mitochondria,  $\Delta\varphi_m$ , redox status, respiratory chain functioning, etc. (iii) Pore opening followed by mitochondrial swelling (the  $k_p$  step) is an “all-or-nothing” event that occurs without any other rate-limiting interme-

diante state(s) that are relevant on the time scale of the overall experiment. In other words, the rate constant  $k_p$  is much faster than the rate-limiting  $k_2$  or the  $\text{Ca}^{2+}$  uptake step  $k_1$ . (iv) When mitochondria undergo  $\text{Ca}^{2+}$ -induced mPT,  $\text{Ca}^{2+}$  is released back to the medium and thus becomes available for uptake by other mitochondria. (v) The rate of formation of  $[\text{MH}]_I$  is a truly rate-limiting step in the reaction sequence (e.g. its rate is slower than the  $\text{Ca}^{2+}$  absorption step ( $k_2 < k_1$ )).

Our proposed model offers several improvements as compared with the earlier models by Massari and others (13, 14, 19). First, the rate of  $\text{Ca}^{2+}$  consumption by mitochondria (the  $k_1$  step) is assumed to be a second order reaction; therefore, the rate changes in proportion with  $[\text{Ca}^{2+}]_{\text{out}}$ . As seen in Fig. 3 (top right),  $[\text{Ca}^{2+}]_{\text{out}}$  can change significantly during the time course of the experiment; therefore, the rate of  $\text{Ca}^{2+}$  uptake can also change significantly. Our second improvement concerns the rate of transient state formation (the  $k_2$  step) triggered in mitochondria by absorbed  $\text{Ca}^{2+}$ . As stated in assumption ii, our model postulates  $k_2$  to be a function of the number of  $\text{Ca}^{2+}$  ions absorbed by mitochondria and thus enables  $k_2$  to change (accelerate) as more  $\text{Ca}^{2+}$  is absorbed by the mitochondria (the model also allows  $k_2$  to be independent of the absorbed  $\text{Ca}^{2+}$  concentration, which occurs when  $n = 0$ ).

Our final and perhaps most significant improvement is that our model describes the autocatalytic role of  $\text{Ca}^{2+}$  in mPT induction. Specifically, the model incorporates the release of  $\text{Ca}^{2+}$  back to the medium from swollen inactive mitochondria, where it becomes available for reuptake by other functionally active mitochondria ( $[\text{MH}]_A$ ). Thus, although the total amount of  $\text{Ca}^{2+}$  ( $[\text{Ca}^{2+}]_T$ ) remains constant, the ratio  $[\text{Ca}^{2+}]_T / [\text{MH}]_A$  as well as the biochemically/physiologically more important ratio  $[\text{Ca}^{2+}]_M / [\text{MH}]_A$  ratio can greatly increase at the end of the mPT process when the population of inactive mitochondria ( $[\text{MH}]_N$ ) increases and the population of active mitochondria ( $[\text{MH}]_A$ ) decreases. This release of  $\text{Ca}^{2+}$  from impaired mitochondria and its secondary reabsorption is unique and central to our model and is sufficient to explain the accelerating rate of the mPT reaction (as seen in Fig. 3, bottom right). By incorporating  $\text{Ca}^{2+}$  reuptake into the model, the model reveals the autocatalytic role of  $\text{Ca}^{2+}$  in mPT induction that has been observed in empirical studies, a feature that has not been captured by previous models. An additional feature of the model is that the form of Equation 1 describing  $k_2$  allows a higher order dependence on  $\text{Ca}^{2+}$ . If  $n$  is  $>1$ , it will tend to make the activation process more cooperative and sharpen the descending portion of the sigmoidal shape of the transition curve.

The earlier kinetic models by Massari and others were developed to describe the mPT process strictly under conditions of a large excess of  $\text{Ca}^{2+}$  in the medium. In this case, free  $\text{Ca}^{2+}$  ( $[\text{Ca}^{2+}]_{\text{out}}$ ) in the medium can be assumed to be constant (because only a small fraction of added  $\text{Ca}^{2+}$  is absorbed by

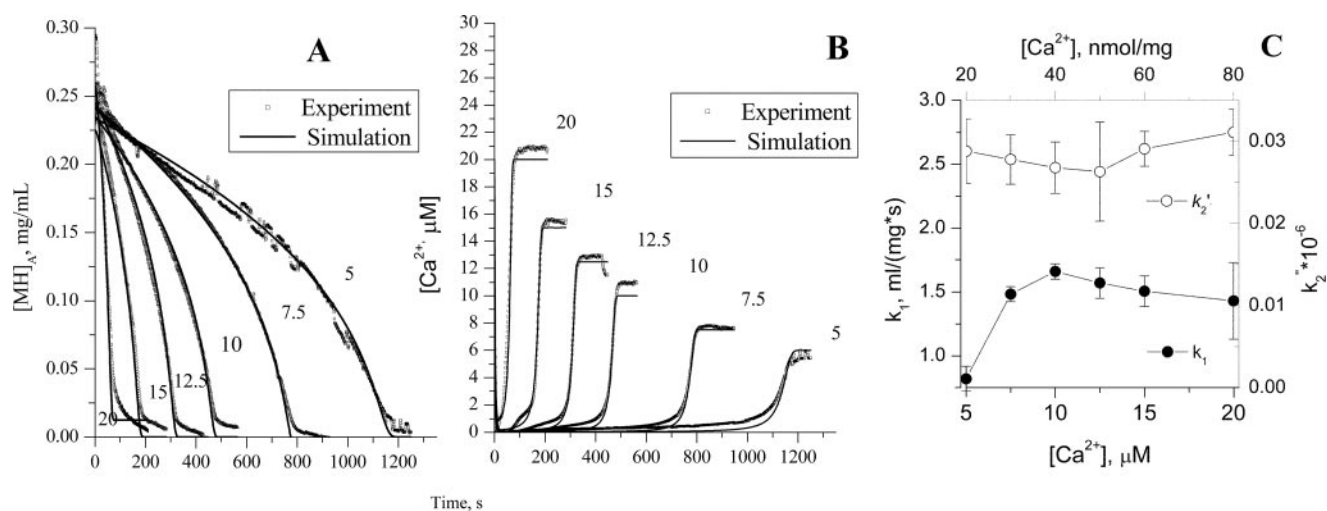


FIGURE 4. Set of rescaled experimental data on mPT in liver mitochondria induced by different concentrations of calcium (open circles). mPT was assigned by simultaneous measurements of four parameters; two ( $Ca$  and  $Swelling$ ) were used in the analysis. Results of numerical simulations are shown as lines. A, kinetic of swelling of mitochondria. B, changes in free (not absorbed by mitochondria)  $[Ca^{2+}]_{out}$ . Concentrations of added  $Ca^{2+}$  (in  $\mu M$ ) are shown as numbers. C, Dependence of kinetic parameters of mPT on  $[Ca^{2+}]_{out}$ . The parameters  $k_1$ ,  $k_2'$ , and  $n$  were determined by fitting of experimental traces with Equations 2 and 3. Because of the complex nature of  $k_2$ , defined in Equation 1, and because  $n$  was found to be constant ( $n = 2.27 \pm 0.03$ ), the parameter  $k_2'$  is shown instead. Note that kinetic parameters in the case of  $5 \mu M$   $[Ca^{2+}]_{out}$  were calculated assuming the presence of  $5.8 \mu M$   $Ca^{2+}$ . For an explanation, see "Experimental Procedures." The S.D. values of the fits are given as error bars. Measurement conditions are the same as in Fig. 2. Time 0 represents the time at which the inducer was added.

mitochondria at any time), and thus effects of the secondary  $Ca^{2+}$  reuptake can be neglected. mPT induction can then be described by a simpler model that involves only first order reactions. This simpler model, however, predicts (and reflects) no delay in the mPT kinetics (because the delay is kinetically irrelevant under these conditions) and thus is not intended to characterize processes underlying pore formation that precede pore opening. Such processes appear to include membrane modifications, such as changes in fluidity (20), as well as modulation of the activity of a number of enzyme cascades participating in mPT opening. As demonstrated below, our new kinetic model is capable of correctly describing the lag phase of the mPT reaction; therefore, it has the potential of providing useful insight into this critical step of the mPT process.

The kinetic model in Scheme 1 can be formulated as a set of two simultaneous differential equations as follows.

$$\frac{d}{dt}[MH]_A = -k_2 \cdot [MH]_A \quad (\text{Eq. 2})$$

$$\frac{d}{dt}[Ca^{2+}]_{out} = -k_1 \cdot [MH]_A \cdot [Ca^{2+}]_{out} + k_2' \cdot [MH]_A \cdot \frac{[Ca^{2+}]_M}{[MH]_A} \quad (\text{Eq. 3})$$

As defined in Equation 1,  $k_2$  is the rate of the intermediate state formation,  $[MH]_p$ , and is assumed to be a function of the number of  $Ca^{2+}$  ions absorbed per mitochondrion. The ratio  $[Ca^{2+}]_M/[MH]_I$  in the last term of Equation 3 is included to account for the hypothesized release of this number of absorbed  $Ca^{2+}$  ions by each inactivated mitochondrion. An additional constraint is also applied; the total concentration of calcium,  $[Ca^{2+}]_T = [Ca^{2+}]_{out} + [Ca^{2+}]_M$ , remains constant during the experiment. This set of nonlinear equations can only be solved numerically. The temporal development of  $[Ca^{2+}]_{out}$

and  $[MH]_A$  can be thus obtained from the equations and then compared with the kinetics observed in the experiment.

The pair of equations (Equations 2 and 3) was solved by using a fixed step Runge-Kutta method implemented in Matlab (The Mathworks®) and applying the initial conditions as specified in the experiment (e.g.  $[MH]_A = 0.25$  (mg of protein/ml) and  $[Ca^{2+}]_T$  varying in each experiment). The computational work was done using a personal computer operated under Windows XP (Microsoft®). A range of  $[Ca^{2+}]_T$  between 5 and 20  $\mu M$  was examined. For concentrations of added  $Ca^{2+}$  below 5  $\mu M$ , no visible mPT reaction was observed on the time scale of our experiments (e.g. after 30 min of incubation). Apparently, the functioning of the mitochondrial respiratory chain was sufficient to compensate for the presence of these low concentrations of  $Ca^{2+}$  for this period of time. For  $Ca^{2+}$  concentrations above 20  $\mu M$ , the mPT occurred without visible lag period; therefore, the resulting kinetics could be analyzed using a simple first order kinetic model described previously (13). Thus, the  $Ca^{2+}$  concentrations examined in this work span the range between those that fail to cause induction and those that cause induction without a lag phase, and the capability(ies) of the new kinetic model was tested in this range. The kinetics for each  $Ca^{2+}$  concentration were simulated by searching for values of  $k_1$ ,  $k_2'$ , and  $n$  that produced the closest fit to the experimental kinetics of both  $[Ca^{2+}]_{out}$  and  $[MH]_A$ . Fig. 4 demonstrates the quality of the fits between experimental and simulated kinetics for several  $Ca^{2+}$  concentrations. The derived values for  $k_1$ ,  $k_2'$ , and  $n$  are summarized in Fig. 4C.

In these simulations, we neglected an additional source of  $Ca^{2+}$ , the isolated mitochondria themselves. For most of the concentrations of added  $Ca^{2+}$  examined, the contribution of the mitochondrially derived  $Ca^{2+}$  did not affect the quality of the fit. The addition of the lowest tested concentration of 5  $\mu M$   $Ca^{2+}$ , however, was associated with an amount of  $Ca^{2+}$

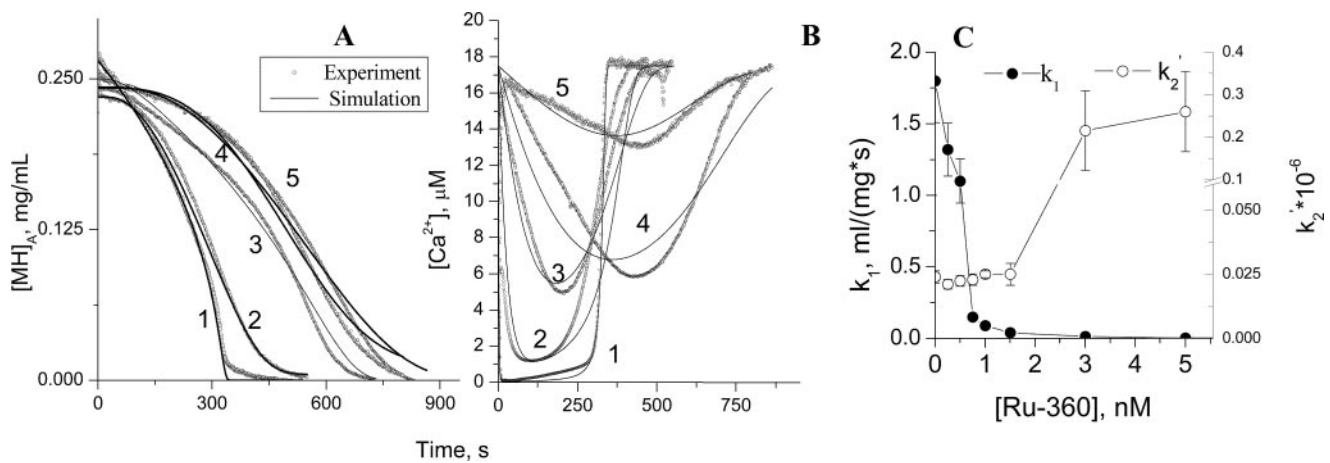


FIGURE 5. Ru-360 blocks  $Ca^{2+}$  uptake and delays the mPT in liver mitochondria induced by 15  $\mu M$  of added calcium. mPT was assigned by simultaneous measurements of four parameters; two ( $Ca$  and Swelling) were used in the analysis. Results of numerical simulations are shown as lines. A, kinetic of swelling of mitochondria. B, changes in  $Ca^{2+}$  fluxes. Concentrations of added Ru-360 for curves 1–5 were 0, 1, 1.5, 3, and 5 nM, respectively. C, kinetic parameters  $k_1$  and  $k_2$  obtained upon fitting of the experimental data  $\Delta$  shown in A and B. Parameter  $n$  was found to be 2.27 in all simulations (not shown). In all experiments, Ru-360 was added prior to the  $Ca^{2+}$ . Time 0 represents the time at which the inducer was added. Other measurement conditions are the same as in Fig. 2.

released to the medium at the end of the reaction that was noticeably higher than the added amount (see Fig. 4B). A better fit to the kinetics was obtained when total  $[Ca^{2+}]_{out}$  was assumed to be 5.5–6  $\mu M$  rather than the actual added concentration (5  $\mu M$ ). This correction derives from an assumption that 0.5–1  $\mu M$  additional  $Ca^{2+}$  was supplied by mitochondria. In a separate experiment, we confirmed that upon the addition of alamethicin, the swollen mitochondria released about 1  $\mu M$  of  $Ca^{2+}$  into the medium as determined using the calibration curve in Fig. 1B.

**Interpretation of the Model**—The quality of the fits in Fig. 4, A and B ( $R^2 > 0.95$ ) demonstrates that the new kinetic model in Scheme 1 is capable of correctly describing the mPT in the range of  $Ca^{2+}$  concentrations used. The extracted dependences of  $k_1$ ,  $k'_2$ , and  $n$  on  $[Ca^{2+}]_T$  provide valuable insight into two steps of the mPT reaction. The rate constant  $k_1$  describes the first step, the  $Ca^{2+}$  uptake by mitochondria. The apparent rate constant  $k_1$  increases proportionally with  $Ca^{2+}$  at low concentrations of  $Ca^{2+}$  (below 10  $\mu M$ ) and becomes concentration-independent at higher  $Ca^{2+}$  concentrations. The increase of  $k_1$  with increasing  $Ca^{2+}$  at low concentrations of  $Ca^{2+}$  is in agreement with previously published data (21) showing that the rate of  $Ca^{2+}$  uptake increases supralinearly upon an increase of  $[Ca^{2+}]_T$ , whereas the activity of  $Ca^{2+}$  efflux pathways remains constant.

The second step in our model, the formation of the transient state  $[MH]_i$ , is described by the two parameters  $k'_2$  and  $n$ . The rate of this step,  $k_2 = k'_2 \times ([Ca^{2+}]_M/[MH]_A)^n$ , depends on the number of  $Ca^{2+}$  ions absorbed by the mitochondria. As discussed above, the rate  $k_2$  can be ascribed to the slowest (rate-limiting) step in the complex chain of reactions induced by an excess of  $Ca^{2+}$  and leading to the formation of  $[MH]_i$ .

The constants  $n$  and  $k'_2$  were found to be unchanged across the  $[Ca^{2+}]_T$  range addressed (*i.e.* the range from noninduction to no lag; Fig. 4C). This finding suggests that, across the range studied, (i) there is likely to be a single reaction or single set of reactions that serves as a rate-limiting step of the mPT; (ii) these constants can be defined, under present conditions, with >90%

precision ( $k_1 = 1.53 \pm 0.12$ ;  $k_2 = 2.76 \times 10^{-7} \pm 0.18 \times 10^{-7}$ ;  $n = 12$ , with constants as mean values  $\pm$  S.E. and  $n$  is the number of experimental runs); and (iii) these constants may be specific, indeed diagnostic, for the conditions studied. The order of the  $Ca^{2+}$  dependence of  $k_2$  was found to be  $n = 2.27 \pm 0.03$  (for all numerical simulations). In the framework of the kinetic model, this indicates that two or more  $Ca^{2+}$  ions are required during this slowest step. The meaning of the fractional value of  $n$  observed under these conditions is currently unknown, but it is most readily explained by postulating pre-existing mitochondrial heterogeneity (*e.g.* preoccupation of a fraction of key sites by  $Ca^{2+}$ ) or branching pathways underlying mPT induction. Assigning the biochemical processes accounted for by these parameters remains for future work (but see below).

These data suggest that these parameters can be readily used as a descriptor of the mPT, providing a qualitative and quantitative characterization of induction. Below, we use this kinetics approach to probe the effect of different inhibitors of the mPT and begin to address the issues raised above.

**Model Validation; Low Concentrations of Ru-360 Delays  $Ca^{2+}$ -induced mPT**—Ru-360, a derivative of ruthenium red, a commonly used inhibitor of the  $Ca^{2+}$  uniporter, was employed to validate our present analysis. Typical doses of ruthenium red and Ru-360 used to prevent mPT are on the order of 1–10  $\mu M$  (22, 23). In our experiments, substantially lower doses of Ru-360 were used in order to reveal the effect of partial inhibition of  $Ca^{2+}$  transport through the uniporter. As shown in Fig. 5A, 1–5 nM concentrations of Ru-360 delayed mPT-associated swelling but also dramatically slowed the rate of  $Ca^{2+}$  uptake by the uniporter (Fig. 5B). (Higher doses of Ru-360 completely abolished  $Ca^{2+}$  transport and mitochondrial swelling).

Simulation of the experimental data (Fig. 5, A and B) in the framework of our model showed that Ru-360 at low-to-moderate concentrations ( $\leq 1.5$  nM) inhibits the rate of  $Ca^{2+}$  uptake (*i.e.* the  $k_1$  step), whereas  $k'_2$  is unaffected (Fig. 5C), as expected from previous reports. At the highest concentration that does not affect  $k'_2$ , Ru-360 further decreased  $k_1$

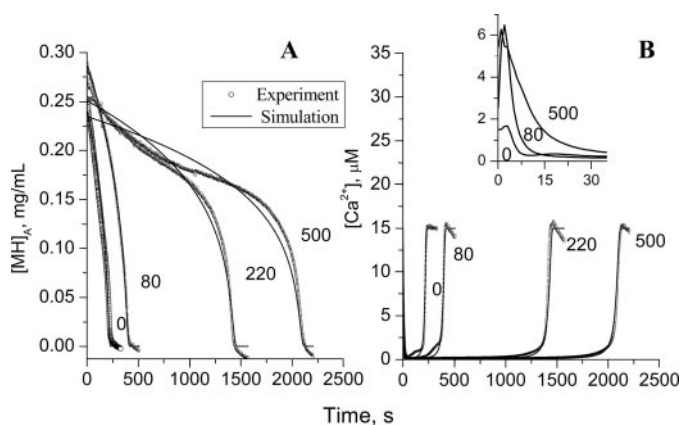


FIGURE 6.  $\text{Mg}^{2+}$  delays  $\text{Ca}^{2+}$ -induced mPT. Calcium ( $15 \mu\text{M}$ ) was added in the presence of different  $[\text{Mg}^{2+}]$  noted as numbers (in  $\mu\text{M}$ ). A, swelling of mitochondria; B, changes in  $\text{Ca}^{2+}$  fluxes. B, inset shows expanded initial kinetics after the addition of  $\text{Ca}^{2+}$ . Results of numerical simulations are shown as lines. Other experimental conditions are the same as in Fig. 2.

45-fold (from 1.8 to 0.04). We estimated  $\text{IC}_{50}$  to be about 0.3 nM for Ru-360 inhibition of the  $k_1$  step, which is close to the previously reported  $\text{IC}_{50} = 0.184 \text{ nM}$  (24).

Unexpectedly, 3–5 nM concentrations of Ru-360 that are well below the normally used concentrations of Ru360 reveal a dramatic increase in  $k'_2$  (Fig. 5C). The result of this increase in  $k'_2$  is to counteract the protective effect of inhibiting the uniporter by uncoupling calcium transport from swelling behavior (curves 4 and 5).

The Ru-360 data provide striking validation of our kinetic model. The ability of the model to describe the parabolic curves in Fig. 5B highlights both the accuracy of our approach and the unique advantages gained through simultaneous simulations across multiple variables (here  $\text{Ca}^{2+}$  and swelling). Indeed, the simultaneous fit of the parabolic curves and the dissociation between  $\text{Ca}^{2+}$  and swelling could not be accommodated by any single component model. In contrast, our two-component model, which was designed to capture the autocatalytic role of  $\text{Ca}^{2+}$  in the mPT, is readily able to accommodate partial inhibition of the uniporter. Furthermore, the model here reveals an additional site for Ru-360 interaction other than the uniporter. Specifically, at concentrations of Ru-360 that are above the  $\text{IC}_{50}$  but below the normally used concentrations of Ru-360,  $k'_2$  also appears to be affected and increases more than 10-fold compared with its value at lower concentrations (Fig. 5C).

**$\text{Mg}^{2+}$  Inhibits  $\text{Ca}^{2+}$ -induced mPT**— $\text{Mg}^{2+}$  has a well known protective effect against  $\text{Ca}^{2+}$ -induced mPT (6, 9). We replicated this effect in the experiments shown in Fig. 6. Kinetic analysis using our new model reveals that  $\text{Mg}^{2+}$  addition is associated with a decrease in the kinetic parameters  $k_1$  and  $k'_2$ , whereas  $n$  increases (Fig. 7). (The decrease in  $k_1$  with increasing  $\text{Mg}^{2+}$  is apparent in the inset to Fig. 6B). Thus,  $\text{Mg}^{2+}$  interferes with  $\text{Ca}^{2+}$  in both processes that lead to mPT.  $\text{Mg}^{2+}$  first slows the uptake of  $\text{Ca}^{2+}$  by mitochondria (Fig. 7A) and then  $\text{Ca}^{2+}$ -induced reactions inside mitochondria (Fig. 7B). (by changing both the rate and concentration order of the activation process). Approximate values of  $\text{IC}_{50}(\text{Mg}^{2+}) = 150 \mu\text{M}$  for the  $k_1$  step and  $\text{IC}_{50}(\text{Mg}^{2+}) = 90 \mu\text{M}$  for the  $k_2$  step can be extracted from the observed dependences (here we define  $\text{IC}_{50}$  as the

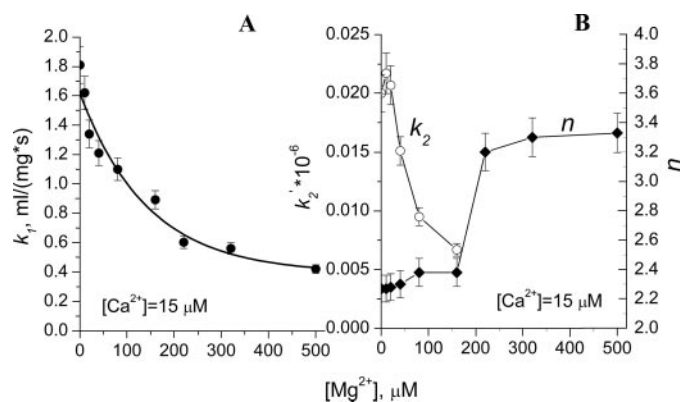


FIGURE 7. Effect of  $\text{Mg}^{2+}$  on the kinetic parameters of  $\text{Ca}^{2+}$ -induced mPT. The parameters were determined by fitting of experimental traces (as in Fig. 6, A and B) with Equations 2 and 3. A, decrease of  $\text{Ca}^{2+}$  uptake rate ( $k_1$ ) in the presence of  $[\text{Mg}^{2+}]$ . B, decrease of  $k_2$  parameter and changes in  $n$  upon increase of  $[\text{Mg}^{2+}]$  in the assay medium. Note that  $k_2$  values were plotted only in the range of  $n = 2.27$  (as in the control sample). The S.D. values of the fits are given as error bars.

$\text{Mg}^{2+}$  concentration at which the rate parameter is reduced by half from its basal value in the absence of  $\text{Mg}^{2+}$ ).

A drastic and sudden change in the order parameter  $n$  occurs at  $\text{Mg}^{2+}$  concentrations higher than  $200 \mu\text{M}$  (Fig. 7B). At low  $\text{Mg}^{2+}$  concentrations, the reaction shows the same order,  $n = 2.27 \pm 0.02$ , as in the absence of  $\text{Mg}^{2+}$ , which suggests that the central rate-limiting reaction is qualitatively conserved, involves  $\text{Ca}^{2+}$ , and is delayed by  $\text{Mg}^{2+}$ . At higher concentrations ( $>200 \mu\text{M}$ ) of  $\text{Mg}^{2+}$ , however, the order parameter increases to  $n = 3.3$ , suggesting that the rate-limiting activation step now involves an additional  $\text{Ca}^{2+}$  ion. Direct comparison of extracted  $k'_2$  is only meaningful within the  $\text{Mg}^{2+}$  ranges in which  $n$  stays the same. Notably, however, within both the low and high concentration ranges, an increase in  $\text{Mg}^{2+}$  concentration results in a decrease in  $k'_2$ .

The current analysis indicates that the protective effect of  $\text{Mg}^{2+}$  against mPT also derives from multiple origins. The addition of  $\text{Mg}^{2+}$  delays mPT onset ( $k'_2$ ) and, at higher concentrations, changes the  $\text{Ca}^{2+}$  stoichiometry ( $n$ ) for mPT formation. In addition,  $\text{Mg}^{2+}$  also delays  $\text{Ca}^{2+}$  uptake ( $k_1$ ; Figs. 6B (inset) and 7A). Nonetheless,  $k_2$  remains the rate-limiting step when  $<200 \mu\text{M}$   $\text{Mg}^{2+}$  is added; thus, our model is a valid description to the mPT inhibition by  $\text{Mg}^{2+}$ .

**Promethazine Protects Mitochondria against  $\text{Ca}^{2+}$ -induced mPT**—Our next application of the new kinetic model was to describe mPT kinetics in the presence of another known mPT inhibitor, the phenothiazine-related antihistamine promethazine, an FDA-approved drug. We recently reported that promethazine blocks mPT *in vitro* and protects primary cerebrocortical neurons from oxygen glucose deprivation in cell culture and mice from middle cerebral artery occlusion-reperfusion-associated infarcts and neurological dysfunction (16). However, little is known about the mechanism of promethazine protection.

Analysis of the experimental kinetics (Fig. 8, A and B) demonstrates that  $k_1$  (i.e. the rate of  $\text{Ca}^{2+}$  uptake) is essentially unaffected by the presence of promethazine (not shown). Promethazine decreases the rate of the second step  $k_2$  by increasing the order of the mPT induction with respect to  $[\text{Ca}^{2+}]$  to  $n = 3$  (Fig. 8C). The simplest interpretation (in terms of our model) is that

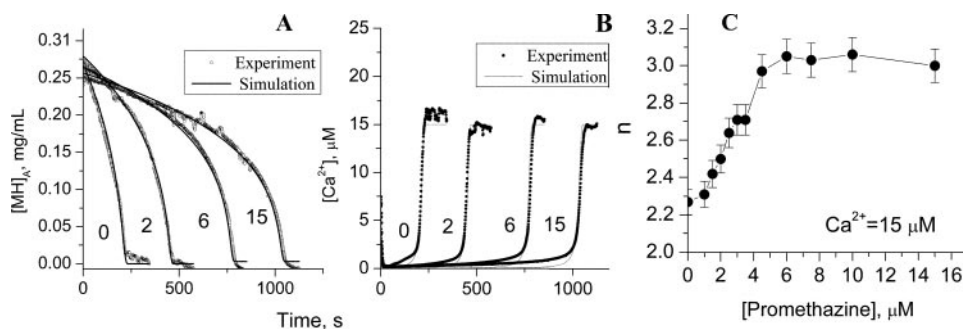


FIGURE 8. **Promethazine delays  $\text{Ca}^{2+}$ -induced mPT.** Calcium ( $15 \mu\text{M}$ ) was added in the presence of different [promethazine] noted as *numbers* (in  $\mu\text{M}$ ). A, swelling of mitochondria; B, changes in  $\text{Ca}^{2+}$  fluxes. Concentrations of added promethazine<sup>+</sup> (in  $\mu\text{M}$ ) are shown as *numbers*. Results of numerical simulations are shown as *lines*. C, dependence of kinetic parameter  $n$  on promethazine concentration upon  $\text{Ca}^{2+}$ -induced mPT. The parameter was determined by fitting of experimental data with Equations 2 and 3. The complex rate constant  $k_2$  is presented through  $n$  (see "Discussion"). The S.D. values of the fits are given as *error bars*. Mitochondria samples were preincubated with different concentrations of promethazine for 1 min and then challenged with  $15 \mu\text{M}$   $\text{CaCl}_2$ . Other experimental conditions are the same as in Fig. 2.

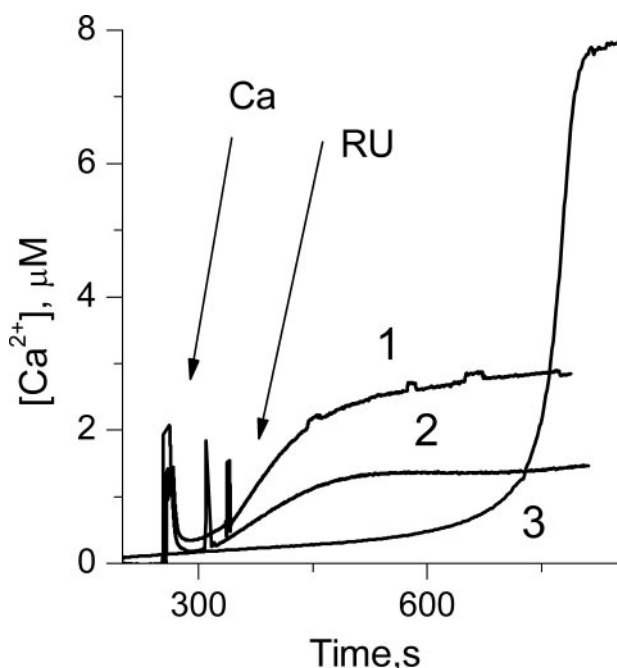


FIGURE 9. **Promethazine inhibits Ru-360-stimulated  $\text{Ca}^{2+}$  release from energized mitochondria.**  $\text{CaCl}_2$  ( $7.5 \mu\text{M}$ ) was added and taken up by mitochondria (*curves 1–3*). The addition of  $20 \text{ nM}$  Ru-360 (*curves 1 and 2*) induced  $\text{Ca}^{2+}$  release from mitochondria and delayed mPT. The presence of  $6 \mu\text{M}$  promethazine (*curve 2*) decreased the rate of  $\text{Ca}^{2+}$  release. *Ca* and *RU* refer to the additions of  $7.5 \mu\text{M}$   $\text{CaCl}_2$  and  $20 \text{ nM}$  Ru-360, respectively. Other experimental conditions are the same as in Fig. 2.

the rate-limiting step in the mPT process now requires three (rather than two)  $\text{Ca}^{2+}$  ions to produce  $[\text{MH}]_i$ . The change in  $n$  indicates a change in the mPT process such that the intermediate state  $[\text{MH}]_i$  contains three instead of two  $\text{Ca}^{2+}$  ions.

The observed change in  $n$  can be used to determine a formal value of  $\text{IC}_{50}$  ( $\sim 3 \mu\text{M}$ ) for promethazine as an mPT inhibitor (here  $\text{IC}_{50}$  is defined as the concentration that induces the median change in the parameter  $n$  from its basal value in the absence of inhibitor). This  $\text{IC}_{50}$  value agrees with the approximate biochemically estimated  $\text{IC}_{50}$ .<sup>3</sup>

<sup>3</sup> I. G. Stavrovskaya, S. V. Baranov, and B. S. Kristal, manuscript in preparation.

Our kinetic model describes the dependence of the rate constant  $k_2$  on  $[\text{Ca}^{2+}]_M$ . Efficiency of  $[\text{Ca}^{2+}]_M$  to induce mPT, however, may be dependent on many factors, such as the mitochondrial redox state,  $\Delta\varphi_m$ , and the presence of mPT modulators, among others. Furthermore,  $[\text{Ca}^{2+}]_M$  itself is regulated in part through  $\text{Ca}^{2+}$  cycling. Since this process is energy-dependent,  $\text{Ca}^{2+}$  cycling contributes to the drop of  $\Delta\varphi_m$  or at least to a need to increase flux through the respiratory chain so as to maintain cycling. Notably, a drop in  $\Delta\varphi_m$  is thought to be among the critical factors contributing to mPT induction. Thus, decreasing

$\text{Ca}^{2+}$  cycling might delay mPT induction. We therefore tested whether promethazine affects  $\text{Ca}^{2+}$  cycling.

As reported above, promethazine does not have any effect on the  $\text{Ca}^{2+}$  uptake rate,  $k_1$ . However, the use of Ru-360 to block  $\text{Ca}^{2+}$  reuptake revealed that promethazine decreased the gradual release of absorbed  $\text{Ca}^{2+}$  into the assay medium (Fig. 9). The lack of detectable swelling suggests that mPT was not involved in this release, implicating other efflux pathways. This experimental observation suggests that promethazine diminished the rate of the  $\text{Ca}^{2+}$  cycling by retarding efflux. Fitting the experimental data in Fig. 9 with one exponent yielded a good fit ( $R^2 > 0.99$ ). These data suggest a possible assignment of  $n$  to the activity of the  $\text{Ca}^{2+}$  efflux pathway(s). Further testing of this mechanism in the context of other inhibitors is in progress.

Thus, the kinetic model was able to describe, both qualitatively and quantitatively, a fundamental difference in the nature of the mechanisms by which Ru-360,  $\text{Mg}^{2+}$ , and promethazine provide protection against the mPT.

## DISCUSSION

Cell death in the presence of pathophysiological  $\text{Ca}^{2+}$  overload (e.g. in stroke) appears associated with mPT induction. We have developed and validated a minimal kinetic model of the mPT in populations of isolated rat liver mitochondria that quantitatively describes  $\text{Ca}^{2+}$ -induced mPT as a sequence of two steps: initiation (which includes initial  $\text{Ca}^{2+}$  uptake) and lag phase (which presumably includes  $\text{Ca}^{2+}$  cycling and pore development). The model was formulated as a pair of simultaneous differential equations, which each relate directly to measurable experimental parameters, specifically fluorescence measurements of  $\text{Ca}^{2+}$  fluxes and mitochondrial swelling, which were in turn assessed using a newly improved optical approach to determine multiple mitochondrial properties simultaneously.

Our model incorporates the autocatalytic nature of  $\text{Ca}^{2+}$  in mPT induction. To our knowledge, this is the first model that simultaneously accounts for the role of the well known  $\text{Ca}^{2+}$  reuptake and swelling in mPT induction. Application of the model is possible because of the high resolution synchronized data provided by the high speed filter wheel-based fluorimeter.

The results reported above address three issues related to understanding the mPT: (i) improvements in measurement methodology; (ii) validation of a kinetic model of the mPT; and (iii) kinetic evidence that Ru-360,  $\text{Mg}^{2+}$ , and promethazine inhibit functionally different phases of the mPT process. We will address each of these subjects in detail below.

**Methodology**—Induction of mPT is associated with temporally linked changes in a broad series of mitochondrial parameters, and these parameters have been observed to change in subtly or overtly different ways after modification of mPT by different inducers or inhibitors. As such, the simultaneous measurement of as many of these parameters as possible could reasonably be expected to enable a more complete understanding of the processes involved. Swelling, for example, is a useful measure of this process in mitochondria isolated from liver but may not be from brain (25–27). Loss of  $\Delta\varphi_m$  may or may not be related to mPT induction. Our recent work has demonstrated the possibility of simultaneously measuring  $\text{Ca}^{2+}$  fluxes and changes in the  $\Delta\varphi_m$  of isolated mitochondria using an ion-selective electrode system. Coupling these electrodes with a Clark-type  $\text{O}_2$ -electrode and a light-emitting diode/photo-diode pair enabled the set-up to simultaneously measure four essential mitochondrial parameters (14). Electrode-based measurement systems, however, are limited by sensor response times as well as chemical properties of the measurement chamber. One example is the practical limitation on the use of certain organic compounds that interfere with the electrode response or permanently contaminate electrodes.

The filter wheel-based fluorimeter employed here enables optical monitoring of four parameters of mitochondrial function that are altered before and during mPT induction: (i) mitochondrial swelling; (ii) NAD(P)H oxidation; (iii)  $\text{Ca}^{2+}$  flux; and (iv)  $\Delta\varphi_m$ . One major advantage of the current system as compared with the previously used potentiometric method is that this system enables measurement of parameters of interest at up to 62.5 Hz (*versus* 0.5 Hz in the previous method (14)). This ability facilitates the measurement of parameters with relatively fast kinetics, such as net  $\text{Ca}^{2+}$  uptake by populations of isolated mitochondria. Filter-based construction enables measurements to be taken from up to eight optical channels and allows independent adjustment of the excitation/emission light intensities for each channel. This enables simultaneous use of dyes with quite different fluorescence intensities.

Our calibration measurements showed a linear dependence of relevant signals on the fraction of intact mitochondria and the level of NAD(P)H oxidation (Fig. 1). A decrease in light scattering has been shown to correlate with the percentage of mitochondria undergoing swelling as a result of mPT (28). Our results are in agreement with earlier publications showing the correlation measured using a conventional fluorescence spectrometer (29).

The Ru-360 experiments provide a direct exemplar of the power of simultaneously monitoring multiple readouts of mitochondrial function. In contrast to many examples where  $\text{Ca}^{2+}$  transport and swelling proceed in apparent lockstep, the data in Fig. 5 show a clear disconnect between these two parameters, a disconnect that we were then able to model using the novel approach described.

**Validating a Kinetic Model of the mPT**—The kinetic model introduced in this work is strictly based on direct measurement data, and retrospective analysis supports the initial assumptions made. Specifically, (i) the kinetic model reflects changes of two parameters that are generally considered to be tightly associated with mPT (swelling and  $\text{Ca}^{2+}$  fluxes). (ii) Each of the kinetic parameters in Scheme 1 is representative of biochemical and/or biophysical processes occurring during mPT induction. (iii) The experimental data were compared with the model to obtain kinetic parameters.

One of the most important features of the model is that it implies a tight mechanistic coupling between swelling and  $\text{Ca}^{2+}$  fluxes. This clearly formulated dependence (Equations 2 and 3) demonstrates that an increase in the rate of swelling increases the rate at which mitochondria release  $\text{Ca}^{2+}$  into the medium, which in turn is taken up by other mitochondria and increases the rate of swelling (autocatalysis). Using this autocatalytic model, it was possible to find kinetic parameters that correctly describe the kinetics of swelling,  $\text{Ca}^{2+}$  uptake, and  $\text{Ca}^{2+}$ -induced  $\text{Ca}^{2+}$  release. In other words, the pure  $\text{Ca}^{2+}$  overload model of mPT used was characterized by assuming strong (mathematical) coupling between  $\text{Ca}^{2+}$  fluxes and swelling. Furthermore, the higher order concentration dependence on  $\text{Ca}^{2+}$  further contributes to continuous acceleration of mPT once an initial “seeding” mass of mitochondria have undergone mPT. Thus, it is possible to use our model to predict the kinetics of any of those processes (*i.e.* swelling,  $\text{Ca}^{2+}$  uptake, or  $\text{Ca}^{2+}$ -induced  $\text{Ca}^{2+}$  release) This feature of our model can also be applied to characterize potential modulators of mPT.

*In vitro*, the most commonly used biochemical model of mPT induction is  $\text{Ca}^{2+}$  overloading. Using the kinetic analysis developed here, we showed that the lag phase of the induction process was correlated with  $[\text{Ca}^{2+}]_T$  in the assay medium (Fig. 4, parameter  $k'_2$ ). Pokhilko *et al.* (12) reached a similar conclusion using a far more sophisticated, bottom-up, primarily theoretical approach that considered the most important processes affecting  $\text{Ca}^{2+}$  homeostasis in mitochondria, such as the functioning of the  $\text{Ca}^{2+}$  uniporter,  $\text{Ca}^{2+}$  antiporters, and  $\text{K}^+$ -dependent processes. Our model, despite lacking many of these specific details of the mPT process, was nonetheless able to correctly capture the  $\text{Ca}^{2+}$  dependence of mPT and predict the detailed  $\text{Ca}^{2+}$  fluxes in a variety of circumstances caused by mPT modifiers. These results suggest that the assumptions we made to solve the kinetic model were correct and demonstrate the utility and power of our simpler model.

In the absence of modifiers, the kinetic parameters that are the major contributors to the delay phase ( $k'_2$  and  $n$ ) remain constant over the range of  $[\text{Ca}^{2+}]$  present in the assay medium, which in our experiments ranged from concentrations that do not appear to ever induce mPT to those that appear to induce mPT without an observable delay. These data suggest that the rate-limiting step of mPT in the pure  $\text{Ca}^{2+}$  overload model is unchanged across this concentration range. In other words, increasing concentrations of  $\text{Ca}^{2+}$  reduce lag by accelerating the same pathways associated with the mPT process rather than by enlisting different processes leading to pore opening. Given the data on mitochondrial calcium interactions gathered over decades, we can speculate with some confidence that the

major factor determining the rate-limiting step of mPT induction is related to  $\text{Ca}^{2+}$  cycling and the ability to maintain the proton gradient in the face of this challenge. The rate of  $\text{Ca}^{2+}$  cycling would, in the early phases of the experimental mPT induction, in turn be related to and limited by both the rate of the  $\text{Ca}^{2+}/\text{H}^{+}$  exchanger and the rate of  $\text{Ca}^{2+}$  appearance in the buffer due to mPT-related release. In the late phases of experimental mPT induction, in contrast, the rate of  $\text{Ca}^{2+}$  cycling would be related to and limited by the rate of  $\text{Ca}^{2+}$  appearance in the buffer due to mPT-related release, the number of remaining mitochondria, and the ability of the respiratory chain of remaining mitochondria to regenerate the proton gradient (which in turn limits uniporter activity at the level of the individual mitochondrion).

**Comparison with Other Models**—Previous models (13), which considered  $\text{Ca}^{2+}$ -induced mPT as a first order kinetic (or, strictly speaking, a pseudo-first order) reaction, focused on only a single response variable. In fact, during the time course of an experiment, the  $[\text{Ca}^{2+}]$  available for uptake undergoes a notable change, from almost zero (when all  $\text{Ca}^{2+}$  is sequestered) to 100% (when the fraction of  $\text{Ca}^{2+}$  taken up by mitochondria is negligible compared with  $[\text{Ca}^{2+}]_T$ ). At the same time, the fraction of active mitochondria decreases from 100 to 0%. These phenomena create a situation that, at the population level, appears as a type of positive feedback, which is reflected in the increasing rate of mitochondrial swelling. Thus, temporal changes in each of the components of the mPT process (mitochondria and calcium) cannot be ignored during modeling of the mPT. Therefore, we considered net  $\text{Ca}^{2+}$  uptake to be a process dependent on both  $[\text{Ca}^{2+}]$  and mitochondria.

This feedback-like  $\text{Ca}^{2+}$  reuptake cycle makes it impossible to find an analytical solution for the  $\text{Ca}^{2+}$ -induced mPT kinetic model. In practice, previous workers have attempted to avoid this complication, using approaches such as focusing on de-energized mitochondria that do not take up  $\text{Ca}^{2+}$  (19) or adding high concentrations of  $\text{Ca}^{2+}$ , such that the process of reuptake of  $\text{Ca}^{2+}$  is negligible relative to the initial uptake (13, 14). We extended the modeling efforts of these groups to address these conditions by applying a numerical approach, which enables use of these systems under more (patho)physiological conditions.

The model we developed can be readily shown to yield kinetic information similar to that generated by Massari's (13) when we examine our model under his conditions and assumptions. Specifically, when high concentrations of  $\text{Ca}^{2+}$  were applied ( $>20\ \mu\text{M}$  in our case), the model predicts incomplete initial  $\text{Ca}^{2+}$  uptake and a nearly instantaneous swelling response (not shown). In this situation, the mPT process can be described as a first order reaction and kinetic analysis could be applied, as was done earlier (13).

Our model focuses on accounting for the aspects of the delay of mPT induction that become limiting when mitochondria are challenged with relatively low concentrations of  $\text{Ca}^{2+}$ . This situation has great physiological and pathophysiological relevance, because extending this delay holds promise in developing therapeutics against a wide series of insults, such as ischemia-reperfusion (6, 7, 30, 31). As shown in several exam-

ples, the model presented here facilitates functional investigation of agents that modulate mPT.

The kinetic parameter  $k_2$  is closely related to the ability of the sequestered  $\text{Ca}^{2+}$  to induce mPT. In our analysis, the value of  $k_2$  itself depends on  $\text{Ca}^{2+}$ . This dependence appears in our analysis as the rate constant  $k'_2$  of step  $k_2$  and parameter  $n$ . By direct analogy with chemical kinetics, in which parameter  $n$  is interpreted as the order of the reaction, we speculate that an increase in  $n$  reflects an increase in the number of mitochondrial components that must interact to lead to mPT induction. Therefore, any increase in  $n$  would be expected to reflect an increase in the ability of mitochondria to resist mPT induction by  $\text{Ca}^{2+}$ , as is seen in the experimental data on  $\text{Mg}^{2+}$  and promethazine shown in Figs. 6–8. The complexity of the events involved in mPT induction makes it difficult to assign  $n$  to any particular mitochondrial process; however, the possibility of calculating  $n$  and then comparing this value across different mPT modulators may enable one to garner information about the relative order/complexity of the events required to induce mPT. The data on  $\text{Mg}^{2+}$  and promethazine provide a practical example.

**Promethazine, Magnesium, and Ru-360 Are Distinguished by Their Effects on mPT Kinetics**—Our kinetic model not only accurately simulates time-dependent changes in mitochondrial physiology during mPT induction but also offers the potential to probe the nature of different inducers and inhibitors of the process of mPT induction in both a qualitative and quantitative manner. The model enables direct testing of whether compounds of interest interfere with  $\text{Ca}^{2+}$  uptake (step  $k_1$ ) or affect the lag phase (step  $k_2$ , parameters  $k'_2$  and  $n$ ). For example, the classical  $\text{Ca}^{2+}$  uniporter inhibitor Ru-360 primarily inhibited mPT by slowing down  $k_1$  ( $\text{Ca}^{2+}$  uptake). In contrast,  $\text{Mg}^{2+}$  inhibited the mPT by slowing down both  $k_1$  and  $k'_2$  and at higher concentrations increasing  $n$ .

$\text{Mg}^{2+}$  and Ru-360 were thus both found by the model to interfere with the  $\text{Ca}^{2+}$  uptake; this prediction is consistent with known inhibition at the phenomenological level of the  $\text{Ca}^{2+}$  uniporter. The uniporter is inhibited by  $\text{Mg}^{2+}$  (8, 32, 33), perhaps because of competition for binding at the  $\text{Ca}^{2+}$  transport site. Ru-360, among the strongest known inhibitors of the uniporter, is not thought to bind to the transport site (24). The kinetic model further reveals that  $\text{Mg}^{2+}$  but not Ru-360 also inhibits  $\text{Ca}^{2+}$ -induced effects at a downstream stage of mPT induction (*i.e.* at a site other than the uniporter). Thus,  $\text{Mg}^{2+}$  works at all three functional sites,  $k_1$ ,  $k_2$ , and  $n$ . The protective effect of  $\text{Mg}^{2+}$  on the  $k_2$  step is concentration-dependent; relatively low concentrations of  $\text{Mg}^{2+}$  decrease  $k'_2$  and do not affect  $n$ . Presumably, this effect relates to competition between the two divalent cations,  $\text{Ca}^{2+}$  and  $\text{Mg}^{2+}$ . On the other hand, high concentrations of  $\text{Mg}^{2+}$  affect  $n$ , which in terms of our analysis reflects an increase in the resistance of mitochondria to  $\text{Ca}^{2+}$ -induced mPT.

Kinetic analysis reveals that promethazine significantly delays the lag phase of mPT by affecting kinetic step  $k_2$  by increasing the parameter  $n$  ( $k'_2$  is functionally irrelevant when  $n$  changes). Studies related to determining the physiological process underlying the protective mechanism of promethazine found that promethazine significantly delays  $\text{Ca}^{2+}$  efflux, which would be predicted to decrease the rate of  $\text{Ca}^{2+}$  cycling.

These observations lead us to tentatively associate reduced  $\text{Ca}^{2+}$  cycling effect with the observed increase of parameter  $n$ . This conceptual linkage is consistent with observations that high concentrations of  $\text{Mg}^{2+}$  also increase  $n$  and affect  $\text{Ca}^{2+}$  efflux. From the viewpoint of inhibitor mechanism studies, our results lead to a working hypothesis that the mechanism of promethazine and high concentrations of  $\text{Mg}^{2+}$  is largely due to decreased  $\text{Ca}^{2+}$  cycling, which preserves mitochondrial energy ( $\Delta\varphi_m$  etc.). In contrast, low  $\text{Mg}^{2+}$  acts both through its effects on the uniporter (based on effects on  $k_1$ ) and through a component of the mPT pathway that is independent of  $\text{Ca}^{2+}/\text{H}^+$  exchange.

**Utility of the Kinetic Modeling Approach**—The modeling approach taken augments and facilitates research on mPT in at least four ways. (i) It provides orthogonal validation/verification of work done using different experimental approaches. The nature of inhibition of Ru-360 as a relatively pure inhibitor of  $\text{Ca}^{2+}$  entry and of  $\text{Mg}^{2+}$  as a more complex inhibitor of multiple  $\text{Ca}^{2+}$ -dependent steps, including entry, had been suggested by investigators using other techniques (6, 9, 24). Our work provides direct experimental support for these models using an orthogonal approach. (ii) It tests hypotheses. The use of our kinetic model of the Ru-360 experiments revealed that decreasing the rate of  $\text{Ca}^{2+}$  uptake in the presence of Ru-360 did not correlate with the rate of mPT induction; this provides a direct experimental argument against the hypotheses that rates of  $\text{Ca}^{2+}$  entry or  $\text{Ca}^{2+}$  concentration are the primary rate-limiting stage in mPT induction (more formally, our model would not have predicted Ru-360 behavior if this hypothesis is valid; see assumption v above). (iii) It provides a new means of generating testable hypotheses. These results of our modeling work further generate the hypothesis that  $\text{Ca}^{2+}$  cycling rather may be the primary rate-limiting stage in mPT induction. This hypothesis remains to be directly addressed but is supported by the promethazine studies. More specifically, the effect of promethazine on  $\text{Ca}^{2+}$  efflux, another hypothesis generated by the model, appears to implicate  $\text{Ca}^{2+}$  efflux (which would reduce cycling), as a potential rate-limiting stage in mPT. (iv) It provides a ready means of quantifying the efficacy of inhibitors of mPT. The application of the model allowed the determination of  $\text{IC}_{50}$  for promethazine protective action and the threshold effect for the target of  $\text{Mg}^{2+}$ . Thus, the experiments with promethazine and  $\text{Mg}^{2+}$  demonstrated the utility of the model to characterize inhibitory action of pharmacologically relevant compounds at both the mechanistic and quantitative realms.

**Conclusion**—We have created and validated a kinetic model of mPT that is expected to aid in the quantitative characterization of mPT induction and the qualitative and quantitative analysis of mPT inhibitors, as empirically demonstrated for  $\text{Mg}^{2+}$  and promethazine. The model may also facilitate determination of the qualitative and quantitative similarity(ies) or difference(s) among potential validated therapeutic targets for inhibition of mPT induction.

## REFERENCES

- Matsumoto, S., Friberg, H., Ferrand-Drake, M., and Wieloch, T. (1999) *J. Cereb. Blood Flow Metab.* **19**, 736–741
- Schinder, A. F., Olson, E. C., Spitzer, N. C., and Montal, M. (1996) *J. Neurosci.* **16**, 6125–6133
- Friberg, H., and Wieloch, T. (2002) *Biochimie (Paris)* **84**, 241–250
- Bernardi, P., Scorrano, L., Colonna, R., Petronilli, V., and Di, L. F. (1999) *Eur. J. Biochem.* **264**, 687–701
- Green, D. R., and Reed, J. C. (1998) *Science* **281**, 1309–1312
- Bernardi, P., Krauskopf, A., Basso, E., Petronilli, V., Blachly-Dyson, E., Di, L. F., and Forte, M. A. (2006) *FEBS J.* **273**, 2077–2099
- Stavrovskaya, I. G., and Kristal, B. S. (2005) *Free Radic. Biol. Med.* **38**, 687–97
- Gunter, T. E., Gunter, K. K., Sheu, S. S., and Gavin, C. E. (1994) *Am. J. Physiol.* **267**, C313–C339
- Zoratti, M., and Szabo, I. (1995) *Biochim. Biophys. Acta* **1241**, 139–176
- Novgorodov, S. A., Guduz, T. I., Milgrom, Y. M., and Brierley, G. P. (1992) *J. Biol. Chem.* **267**, 16274–16282
- Dolder, M., Walzel, B., Speer, O., Schlattner, U., and Wallimann, T. (2003) *J. Biol. Chem.* **278**, 17760–17766
- Pokhilko, A. V., Ataullakhanov, F. I., and Holmuhamedov, E. L. (2006) *J. Theor. Biol.* **243**, 152–169
- Massari, S. (1996) *J. Biol. Chem.* **271**, 31942–31948
- Krasnikov, B. F., Zorov, D. B., Antonenko, Y. N., Zaspas, A. A., Kulikov, I. V., Kristal, B. S., Cooper, A. J., and Brown, A. M. (2005) *Biochim. Biophys. Acta* **1708**, 375–392
- Zhu, S., Stavrovskaya, I. G., Drozd, M., Kim, B. Y., Ona, V., Li, M., Sarang, S., Liu, A. S., Hartley, D. M., Wu du, C., Gullans, S., Ferrante, R. J., Przedborski, S., Kristal, B. S., and Friedlander, R. M. (2002) *Nature* **417**, 74–78
- Stavrovskaya, I. G., Narayanan, M. V., Zhang, W., Krasnikov, B. F., Heemskerk, J., Young, S. S., Blass, J. P., Brown, A. M., Beal, M. F., Friedlander, R. M., and Kristal, B. S. (2004) *J. Exp. Med.* **200**, 211–222
- Scaduto, R. C., and Grotyohann, L. W. (1999) *Biophys. J.* **76**, 469–77
- Rajdev, S., and Reynolds, I. J. (1993) *Neurosci. Lett.* **162**, 149–152
- Dedov, V. N., Demin, O. V., Chernyak, V. Y., and Chernyak, B. V. (1999) *Biochemistry (Mosc.)* **64**, 809–816
- Ricchelli, F., Jori, G., Gobbo, S., Nikolov, P., and Petronilli, V. (2005) *Int. J. Biochem. Cell Biol.* **37**, 1858–1868
- Nicholls, D. G. (2005) *Cell Calcium* **38**, 311–317
- Paradies, G., Petrosillo, G., Pistolesi, M., Di, V. N., Federici, A., and Rugiero, F. M. (2004) *Circ. Res.* **94**, 53–59
- Zhang, S. Z., Gao, Q., Cao, C. M., Bruce, I. C., and Xia, Q. (2006) *Life Sci.* **78**, 738–745
- Matlib, M. A., Zhou, Z., Knight, S., Ahmed, S., Choi, K. M., Krause-Bauer, J., Phillips, R., Altschuld, R., Katsube, Y., Sperelakis, N., and Bers, D. M. (1998) *J. Biol. Chem.* **273**, 10223–10231
- Andreyev, A. Y., Fahy, B., and Fiskum, G. (1998) *FEBS Lett.* **439**, 373–376
- Brustovetsky, N., and Dubinsky, J. M. (2000) *J. Neurosci.* **20**, 8229–8237
- Kristian, T., Weatherby, T. M., Bates, T. E., and Fiskum, G. (2002) *J. Neurochem.* **83**, 1297–1308
- Hunter, D. R., and Haworth, R. A. (1979) *Arch. Biochem. Biophys.* **195**, 453–459
- Hansson, M. J., Mansson, R., Mattiasson, G., Ohlsson, J., Karlsson, J., Keep, M. F., and Elmer, E. (2004) *J. Neurochem.* **89**, 715–729
- Griffiths, E. J., and Halestrap, A. P. (1995) *Biochem. J.* **307**, 93–98
- Halestrap, A. P., Kerr, P. M., Javadov, S., and Suleiman, M.-S. (2001) in *Mitochondria in Pathogenesis* (Lemasters, J. J., and Nieminen, A.-L., eds) pp. 177–200, Kluwer Academic/Plenum Publishers, New York
- Crompton, M., and Roos, I. (1985) *Biochem. Soc. Trans.* **13**, 667–669
- Nicholls, D., and Akerman, K. (1982) *Biochim. Biophys. Acta* **683**, 57–88

**Kinetic Model for  $\text{Ca}^{2+}$ -induced Permeability Transition in Energized Liver Mitochondria Discriminates between Inhibitor Mechanisms**

Sergei V. Baranov, Irina G. Stavrovskaya, Abraham M. Brown, Alexei M. Tyrishkin and Bruce S. Kristal

*J. Biol. Chem.* 2008, 283:665-676.

doi: 10.1074/jbc.M703484200 originally published online October 25, 2007

---

Access the most updated version of this article at doi: [10.1074/jbc.M703484200](https://doi.org/10.1074/jbc.M703484200)

Alerts:

- [When this article is cited](#)
- [When a correction for this article is posted](#)

[Click here](#) to choose from all of JBC's e-mail alerts

This article cites 32 references, 10 of which can be accessed free at <http://www.jbc.org/content/283/2/665.full.html#ref-list-1>